PHYSICAL REVIEW B **104**, 134437 (2021)

Magnon polarons in the van der Waals antiferromagnet $FePS_3$

D. Vaclavkova,[1,*] M. Palit,[2,*] J. Wyzula,[1] S. Ghosh,[2] A. Delhomme,[1] S. Maity,[2] P. Kapuscinski,[1,3] A. Ghosh,[2]
M. Veis,[1,4] M. Grzeszczyk,[1,5] C. Faugeras,[1] M. Orlita,[1,4] S. Datta,[2,†] and M. Potemski[1,5,‡]
[1] *Laboratoire National des Champs Magnétiques Intenses, LNCMI-EMFL, CNRS UPR3228, Université Grenoble Alpes, Université Toulouse, Université Toulouse 3, INSA-T, Grenoble and Toulouse, France*
[2] *School of Physical Sciences, Indian Association for the Cultivation of Science, 2A & B Raja S. C. Mullick Road, Jadavpur, Kolkata 700032, India*
[3] *Department of Experimental Physics, Wroclaw University of Technology, Wybrzeze Wyspianskiego 27, 50-370 Wroclaw, Poland*
[4] *Institute of Physics, Charles University, Ke Karlovu 5, Prague, 121 16 Czech Republic*
[5] *Institute of Experimental Physics, Faculty of Physics, University of Warsaw, ul. Pasteura 5, 02-093 Warszawa, Poland*

(Received 24 August 2021; accepted 18 October 2021; published 29 October 2021)

The hybridization of magnons (spin waves) with phonons, if sufficiently strong and comprising of long wavelength excitations, may offer a new playground when manipulating the magnetically ordered systems with light. Applying a magnetic field to a quasi-two-dimensional antiferromagnet, $FePS_3$, we tune the magnon-gap excitation to coincide with the initially lower-in-energy phonon modes. Hybrid magnon-phonon modes, the magnon polarons are unveiled with the demonstration of a pronounced avoided crossing between the otherwise bare magnon and phonon excitations. The magnon polarons in $FePS_3$ are traced with Raman scattering experiments. However, as we show, they also couple directly to terahertz photons, evoking their further explorations in the domain of antiferromagnetic optospintronics. The magnon-phonon coupling is also discussed as a possible reason of the magnon mode splitting observed in the absence of a magnetic field.

DOI: 10.1103/PhysRevB.104.134437

I. INTRODUCTION

Research on magnetic solids recently gave rise to a plethora of emerging domains of study, which are motivated by the scientific curiosity to uncover new phenomena and triggered by the possible design of, optional to electronic, spintronic devices [1]. Among current trends in the spintronic developments, there are attempts to exploit antiferromagnetic materials [2] (instead of ferromagnets) to work with two-dimensional systems [3,4], as well as attempts to manipulate magnetically ordered solids with light [5]. These ideas have stimulated our magnetooptical studies of the representative layered antiferromagnet $FePS_3$, in which the characteristic magnon-gap excitation appears at a significantly high frequency of a few terahertz [6,7]. Both the antiferromagnetic order and magnon excitation may survive at the nanoscale, down to the monolayer limit [8,9].

Magnons (spin waves) and phonons (lattice vibrations) are two relevant, low-energy excitations in magnetically ordered systems. The coupling between these modes, central for the present work, has been a subject of numerous theoretical and experimental studies in various ferromagnetic [10,11], antiferromagnetic [12,13], ferrimagnetic [14,15], as well as in multiferroic [16] materials. Coupling between magnons and phonons affects the dynamical and optical properties of these quasiparticles and appears to be of special importance in emerging areas, such as spin caloritronics [17,18] or magnon spintronics in conjunction with new developments in terahertz (THz) technology [19,20].

Coupled magnon-phonon modes, the magnon-polarons, are best evidenced by the observation of the repulsion (avoided crossing) of the otherwise bare phonon and magnon excitations when they are brought to coincide. Such concurrency is customarily expected when the (strongly) linearly dispersing acoustic phonons cross the quadratically dispersing magnons and/or when the dispersing magnons intersect the weakly dispersing (optical-like) phonons, notably, at certain nonzero k wave vectors in both cases. Magnon polarons can then be evidenced with neutron scattering experiments and/or techniques of surface acoustic waves, both providing an access to $k \neq 0$ excitations [11,21–23]. Magnon and phonon excitations can also be probed by means of optical techniques, which are easily operational in conjunction with the application of high magnetic fields. Such methods provide an access to yet another regime, to substantiate evidence of a possible coupling between the $k = 0$ magnon and phonon modes with dispersions that do not cross at any wave vector.

Here we unveil the magnon polarons in the $FePS_3$ antiferromagnet with optical spectroscopy experiments, magneto-Raman scattering, and far-infrared/terahertz (FIR/THz) magnetotransmission measurements, thus naturally probing $k = 0$ excitations. By applying a magnetic field, we split the magnon-gap excitation into two components and drive the lower energy one to intersect the three characteristic Raman- and FIR-active phonon modes, but instead, we observe a series of pronounced anticrossing events. The analysis of the observed anticrossing pattern allows us to estimate the strength of the magnon-phonon coupling in the limit of the magnetic

---

[*] These authors contributed equally to this work.
[†] subhanano@gmail.com
[‡] marek.potemski@lncmi.cnrs.fr

material in which the magnon mode is coupled to lower-in-energy $k = 0$ phonons. We propose that this coupling alters the optical selection rules for magnon and phonon excitations, which, in particular, implies their effective activation with THz photons. The present work complements the previous [24] and very recent [25] magneto-Raman scattering studies of the $FePS_3$ antiferromagnet with, in particular, the far-infrared magnetospectroscopy data and observation of the zero-field splitting of the magnon gap, this splitting is likely also induced by the magnon-phonon coupling.

Although $FePS_3$ is among the best-known layered antiferromagnets within the large family of transition metal phosphorus trichalcogenides (TMPT) [26], the exact rules governing the spin ordering in this material continue being revisited [7,27–32]. This includes very recent reports invoking the possible effects of spin-lattice coupling [33,33]. Below the Néel temperature of $T_N = 120$ K, $FePS_3$ is generally considered as a good example of a two-dimensional antiferromagnet [7,27–32], even in its bulk form, which is composed of weakly bound, via van der Waals forces, layers with Fe^{2+} ($S = 2$) spins arranged on a honeycomb lattice [26,34]. The interlayer spin-spin exchange terms are weak and the antiferromagnetic order, with Fe^{2+} spins aligned along the direction perpendicular to the layers plane, is largely governed by intralayer exchange integrals and the strong term of the single Fe^{2+} ion anisotropy [31]. This last term justifies the Ising-type notion for antiferromagnetism in $FePS_3$ [7,27–32]. It is also the reason for the relatively large energy of the magnon gap, the zero wave vector ($k = 0$) excitation of the lower-energy branch of the spin-waves, in this material. The spin-wave/magnon dispersion relations in $FePS_3$ have been widely studied with neutron scattering [7,30–32]. The magnon gap in this antiferromagnet at low temperature has been identified in Raman scattering experiments with a characteristic signature at $E_M \approx 122\ \mathrm{cm}^{-1}$ [6,24].

II. EXPERIMENTAL DETAILS

The investigated samples consisted of relatively thick flakes (thickness of ~1–10 μm) extracted from bulk $FePS_3$ crystals and deposited on Si/SiO_2 or Si substrates. The surfaces of the flakes have been "cleaned" by the "exfoliation" method before each experimental run to obtain a surface with good optical quality. Either commercially available (HQ Graphene) or home-grown $FePS_3$ crystals were utilized. The second type of crystals were grown by the chemical vapor transport method in two zone furnaces following an established method [35]. All samples have been initially tested with room temperature Raman scattering measurements, and they all showed practically the same characteristics.

The temperature-dependent Raman scattering response was measured at zero magnetic field in a continuous flow cryostat mounted on *x*-*y* motorized positioners. The sample was placed on the cold finger of the cryostat and excited with the 515-nm line of a continuous-wave laser diode. The excitation light was focused by means of a 50× long-working distance objective with a 0.5 numerical aperture producing a spot of about 1 μm and the scattering signal was collected via the same objective. Low-temperature magneto-Raman experiments were performed in the back-scattering configuration with the magnetic field applied perpendicularly to the *ab*-plane of our sample. We used the Faraday geometry, i.e., the magnetic field is parallel to the light propagation direction. Measurements were carried out with magnetic fields up to 30 T using a free-beam-optics arrangement. The sample was placed on top of a *x*-*y*-*z* piezostage (kept in gaseous helium at $T = 4.2$ K), inserted into a magnet and was excited using a 515.1-nm line of a continuous wave laser diode (2.41-eV photon energy). The emitted light was dispersed with a 0.7-m-long monochromator and detected with a CCD camera.

Far-infrared transmission experiments were carried out on a macroscopic $FePS_3$ bulk sample (surface size 10 mm^2) which was kept in the He exchange gas at the temperature of $T = 4.2$ K and placed in a superconducting solenoid (magnetic field up to 18 T) or a resistive coil (magnetic field up to 34 T). The magnetic field was oriented perpendicular to the *ab*-plane of the $FePS_3$ crystal. To measure infrared magnetotransmission, the radiation from a globar source was modulated by a Bruker Vertex 80v Fourier-transform spectrometer, delivered to the sample via light-pipe optics and detected by a composite bolometer placed directly behind the sample. All measurements were performed in the Faraday geometry. The presented transmission spectra were normalized by the transmission of a 1-mm pinhole measured at each magnetic field, thus correcting for magnetic-field-induced variations in the response of the bolometer.

III. EXPERIMENTAL RESULTS

With the results presented in Fig. 1(a), we recall the temperature evolution of the Raman scattering response typically observed in $FePS_3$ crystals [6,8,24,36,37]. The F_i ($i = 1, 2, 3, 4$) features observed above 200 cm^{-1} are largely due to molecular-like vibration of the $(P_2S_6)^{4-}$ anion unit (which together with two Fe^{2+} cations form the simplified unit cell of $FePS_3$) and are pretty common for all TMPT compounds [38,39]. Instead, the Raman scattering peaks seen at lower energies (P_i features) are expected to be due to phonons which include the vibration of Fe^{2+} ions [8,38] while the M feature is now well recognized [24] as due to the magnon-gap excitation. As previously reported [6,8,24] and illustrated in Fig. 1(a), the magnon peak M as well as all P_i peaks are sensitive to the magnetic ordering: when temperature is raised above the Néel temperature of $T_N \approx 120$ K, the intensity of the P_4 resonance drops down abruptly, whereas P_i (i = 1,2,3) and M peaks merge together into a broad P_0 feature. The P_4 peak is commonly associated to a A_g/B_g phonon from the center of the Brillouin zone of the $FePS_3$ crystal [8,24,37,38,40,41]. Instead, the identification of phonons associated with P_i (i = 0,1,2,3) resonances is less conclusive and we will comment more on this issue later on.

In the following we focus our attention on the low-energy spectral range (60–180 cm^{-1}) and low-temperature regime (4.2 K) and examine the Raman scattering and far-infrared transmission spectra of our $FePS_3$ crystal, measured as a function of the magnetic field applied perpendicularly to the layer planes, i.e., along the direction of Fe^{2+} ions' spin alignment. The results of magneto-Raman scattering measurements are illustrated in Fig. 1(b). In accordance to the previous study performed at low magnetic fields [24], the very first effect of the application of a magnetic field is the splitting of the magnon peak into two M_+ and M_-

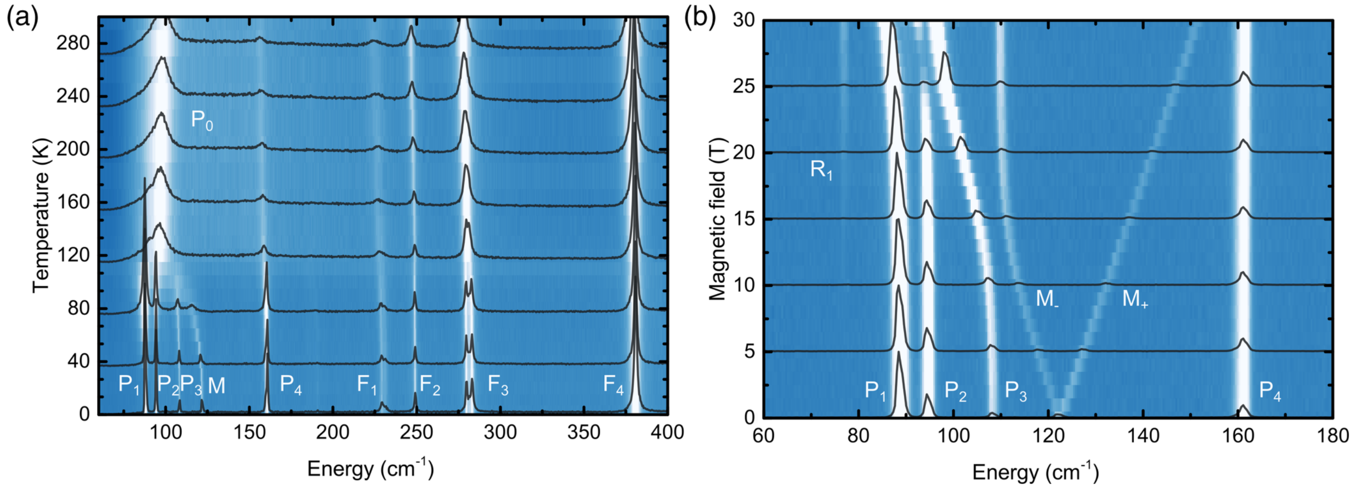

FIG. 1. (a) False-color map of the Raman scattering response of FePS$_3$ antiferromagnet, together with a few selected characteristic spectra, measured as a function of temperature in the range from 4.2 K up to 300 K. P_i ($i = 1, \dots, 4$) and F_i ($i = 1, \dots, 4$) resonances are due to phonon modes and the M-feature corresponds to the magnon-gap excitation. (b) False-color map of the evolution of the low-temperature ($T = 4.2$ K) magneto-Raman scattering response of FePS$_3$ with an applied magnetic field oriented perpendicular to the plane of the layers, together with a few selected spectra, in the spectral region from 60 to 180 cm^{-1}. The coupling between the lower magnon branch M_- and three P_i ($i = 1, \dots, 3$) phonon modes is clearly observed. An additional R_1 phonon mode is activated at high magnetic fields. The energy of the upper M_+ magnon branch smoothly develops with the magnetic field and does not reach the energy of the P_4 phonon in the range of magnetic fields investigated.

components. This energy splitting, approximately linear with the magnetic field (B) in the range of low fields, scales as $2g\mu_B B$ where μ_B stands for the Bohr magneton and, to the first approximation, we find $g \approx 2$ for the effective g-factor, in line with the previous report [24].

The present work highlights the effects observed at high magnetic fields, when the M_- magnon branch is tuned in the spectral range of three low energy $P_i = 1{,}2{,}3$ phonons. As can be seen in Fig. 1(b), the M_- magnon excitation does not intersect any of the P_1, P_2, and P_3 phonons and instead a characteristic pattern of avoided crossing events is observed, in line with recent high-field magneto-Raman study [25]. A simple inspection of the raw data leads us to conclude that the M_- magnon effectively couples to all three P_1, P_2, and P_3 phonons. Besides that, we observe at high magnetic fields (above 14 T) the activation of an additional Raman scattering peak, presumably due to another phonon excitation. The energy position of this additional excitation [marked as R_1 in Fig. 1(b)] does not, however, change with the magnetic field, which prevents us to firmly conclude about its potential strong coupling to the magnon mode. As for the upper M_+ component of the magnon mode, we note its smooth blue shift, approximately linear with the magnetic field. There are no Raman active phonon modes in the spectral range covered by the M_+ magnon component, which only approaches the P_4 phonon at the highest available magnetic fields, but is still not sufficiently close to let us conclude about their possible hybridization. It is still worth noting that the extrapolated crossing of the M_+ magnon branch and the P_4 phonon is expected at $B \approx 40$ T, that is, at the field strength at which the phase transition of the FePS$_3$ ground state has been recently anticipated from magnetization measurements [33].

The results presented in Fig. 2 demonstrate that several excitations among those traced with Raman scattering do also directly couple to light, giving rise to absorption resonances observed in FIR magnetotransmission measurements, which is an experimental technique different from Raman scattering used in previous magnetooptical studies [24,25]. Tracking these resonances (minima/dips in transmission spectra) as a function of the magnetic field we are able to reproduce the characteristic pattern of avoided crossings of the M_- magnon branch with the P_1, P_2, and P_3 phonons. In contrast to M_-/M_+ and to the P_3 excitations that can be clearly

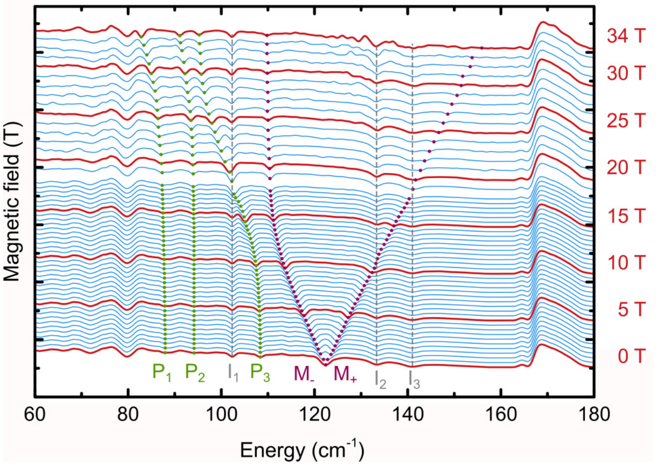

FIG. 2. Low-temperature ($T = 4.2$ K) far-infrared transmission spectra for selected values of the magnetic field applied perpendicular to the layer planes, in the spectral region 60–180 cm^{-1}. Transmission minima denoted as P_i ($i = 1, \dots, 3$) and M_+/M_- have their counterparts in resonances observed in Raman scattering spectra. I_i ($i = 1, \dots, 3$) transitions are only visible in FIR transmission spectra. The pronounced minimum at ~ 80 cm^{-1} is due to absorption resonance in the polyethylene foil used in our experimental setup to filter the high-frequency radiation.

TABLE I. (Upper part) Characteristic energies of resonances observed in Raman scattering (R) and FIR transmission (IR) spectra measured in the absence of magnetic field. (Bottom part) Set of parameters ("bare" energies, coupling constants, and "bare" g-factor) used to reproduce the magnetic field evolution of hybrid magnon-phonon modes (see Fig. 3).

	Coupled modes				Other resonances				
	$\mathrm{M_{agnon}}$	P_1	P_2	P_3	R_1	I_1	I_2	I_3	P_4
Experiment ($B = 0$ T)									
Energy (cm^{-1})	122.0	88.6	94.6	108.5	77.1	102.3	133.3	141.0	161.0
Activity	R/IR	R/IR	R/IR	R/IR	R	IR	IR	IR	R
Modelling for g-factor $= 2.15$									
Energy (cm^{-1})	121.2	89.6	95.0	109.8					
Coupling (cm^{-1})		3.6	2.4	3.1					

observed at anyu value of the magnetic field, the transmission minima related to P_1 and P_2 phonons are rather weakly pronounced at low magnetic fields. They are barely visible in the raw data, but still present even in the spectrum measured in the absence of a magnetic field as deduced when examining the measured magneto-transmission response in more details (see Ref. [42]). On the other hand, the transmission minima, marked as I_1, I_2, and I_3 in Fig. 2 are assigned to other absorption resonances in the FePS$_3$ crystal. These resonances are not Raman active and do not couple to magnon modes (cross either M_- or M_+ magnon branch) and we also note that the R_1 and P_4 resonances, otherwise observed in Raman spectra, are not optically active, not visible in magnetotransmission spectra. For the sake of completeness, let us note that another, relatively weak, spectral feature with the antiferromagnetic-resonance-like splitting appears in the FIR magnetotransmission response at higher energies (around 318 cm^{-1}, see Fig. S3 in Ref. [42]). We assign this mode, in agreement with neutron scattering experiments [31], to the $k = 0$ excitation of the upper magnon mode, expected in antiferromagnets with four moments in the magnetic unit cell. Nevertheless, as we checked, this upper magnon mode is hardly apparent in the Raman scattering response.

The P_1, P_2, and P_3 phonon modes which couple to the magnon excitation are not easily identifiable and this also applies to other (R_1, I_1, I_2, I_3) resonances observed in our spectra. All these resonances are traced with optical experiments and are thus naturally associated to Γ-point excitations of FePS$_3$ in its antiferromagnetic phase. However, even for those basic phonons, no consensus exists between different reports of the calculated phonon dispersions in FePS$_3$ [8,39–41,43]. All these reports predict the presence of only very few Γ-phonons in the low-energy range (60–180 cm^{-1}), when considering the crystal in the paramagnetic phase. In addition to the P_4 Raman peak, only the P_0 feature observed at high temperatures [see Fig. 1(a)] are commonly associated with the calculated phonon of the A_g/B_g or E_g symmetry [8,39–41,43]. A specific broadening effect and/or an unresolved multicomponent character of the P_0 feature remains to be clarified. The unit cell of the FePS$_3$ crystal is, however, enlarged in the magnetically ordered phase, in the direction across as well as along the planes [6,8]. The appearance of multitude of optically active low-energy phonons in the antiferromagnetic phase of FePS$_3$ is expected to be a consequence of the zone folding, in particular of the M-point onto the Γ-point. Apparent phonon energies maybe also affected by an additional deformation of the unit cell of FePS$_3$ at low temperatures [44]. Regrettably, the available results [8,39] of calculated phonon modes in the antiferromagnetic phase of FePS$_3$ do not permit a definite identification of the observed resonances. In any case, the $P_i = 1{,}2{,}3$ phonon modes being central for the present work must be associated with the in-plane motion of Fe^{2+} ions, as they effectively couple to the innately in-plane spin-waves in FePS$_3$. Several Raman-active phonon modes with such symmetry have been predicted to appear in the energy range 70–100 cm^{-1}, in calculations limited to a single FePS$_3$ layer [8]. These optical-like and/or "folded" phonons are not expected to cross the magnon excitation at any k-vector. Their hybridization with the magnon mode is hardly visualized with, for example, conventional neutron scattering experiments, but possible in our studies profiting of the application of magnetic fields [45]. Anticipating new theoretical approaches to calculate the phonon spectra of the FePS$_3$ antiferromagnet, we list, in Table I, the characteristic energies of resonances as they appear in the low-energy range of the measured Raman and far-infrared absorption spectra. Attempts have been also undertaken to measure the magneto-Raman scattering spectra of FePS$_3$ in the configuration of the magnetic field applied along the crystal planes (Voigt geometry). The results of such experiments are inspiring (see Fig. S4 in Ref. [42]), although hardly conclusive since surfaces of our crystals are not perfectly flat, prevents the arrangement of a well-defined Voigt geometry (remaining out-of-plane component of the magnetic field).

IV. THEORETICAL MODELING OF HYBRID MAGNON-PHONON MODES

The effects of magnon-phonon coupling, clearly apparent even in our raw magneto-spectroscopy data [see Fig. 1(b)], are now examined in more detail. The central positions of the Raman scattering peaks and the infrared transmission dips associated with the P_1, P_2, P_3, and M_+/M_- resonances are plotted as a function of the magnetic field, in Fig. 3. To reproduce these data, we refer to a generic theoretical approach to the problem of magnon-phonon coupling [12,46] which, in its complete form, accounts for possible interactions between all relevant (dispersing with wave vector k) branches of magnon and phonon modes present in a magnetically ordered system overall described within the Heisenberg formalism [31]. This general approach is here simplified down to a phenomenological model. We neglect the modes' dispersions and impose a

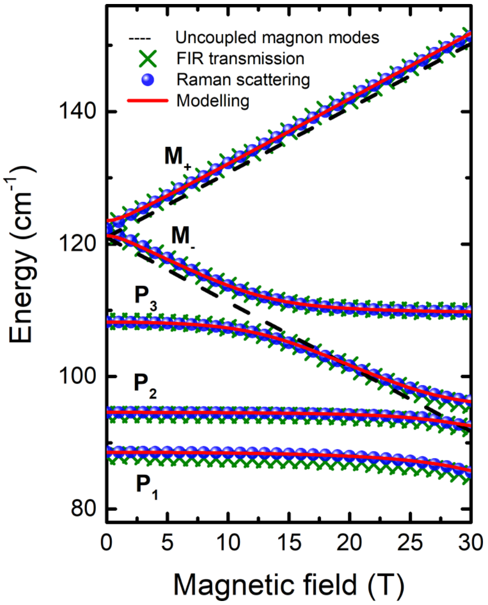

FIG. 3. Magnetic field dependence of the energy positions of hybrid magnon-phonon modes. Full circles represent the experimental data extracted from magneto-Raman scattering measurements. These data are reproduced with solid lines, following the theoretical modeling described in the text. Crosses account for the energy positions of transitions observed in FIR transmission spectra. The resonances observed in Raman scattering and FIR transmission spectra overlap within the experimental error. Dashed lines show the field dependence of energy positions of magnon modes without coupling to phonons.

coupling only between $k = 0$ excitations. Furthermore, only the interactions which clearly appear in our data are considered, i.e., the interaction between (M_+/M_-) magnon modes and three P_1, P_2, and P_3 phonon excitations. All other phonon modes, as well as the upper magnon mode at significantly higher energy (~318 cm^{-1}) have been neglected. In its matrix form, the resulting magnon-phonon interaction Hamiltonian is then given by

$$H = X^\dagger H' X, \tag{1}$$

where

$$X = \left[\alpha_{M_+}, \alpha_{M_-}, \zeta_{P_1}, \zeta_{P_2}, \zeta_{P_3}, \alpha^\dagger_{-M_+}, \alpha^\dagger_{-M_-}, \zeta^\dagger_{-P_1}, \zeta^\dagger_{-P_2}, \zeta^\dagger_{-P_3}\right] \tag{2}$$

is a vector composed of annihilation and creation bosonic operators α_{M_+}, α_{M_-}, ζ_{P_1}, ζ_{P_2}, ζ_{P_3} associated, correspondingly, with the magnetically split magnon gap excitation α_{M_+}, α_{M_-}, and three (dispersionless) P_1, P_2, and P_3 phonons

$$H' = \begin{bmatrix} F & G \\ G & F, \end{bmatrix}, \tag{3}$$

where

$$F = \begin{bmatrix} E^0_{M_+} & 0 & \lambda_1 & \lambda_2 & \lambda_3 \\ 0 & E^0_{M_-} & \lambda_1 & \lambda_2 & \lambda_3 \\ \lambda_1 & \lambda_1 & E^0_{P_1} & 0 & 0 \\ \lambda_2 & \lambda_2 & 0 & E^0_{P_2} & 0 \\ \lambda_3 & \lambda_3 & 0 & 0 & E^0_{P_3} \end{bmatrix}, \tag{4}$$

and

$$G = \begin{bmatrix} 0 & 0 & \lambda_1 & \lambda_2 & \lambda_3 \\ 0 & 0 & \lambda_1 & \lambda_2 & \lambda_3 \\ \lambda_1 & \lambda_1 & 0 & 0 & 0 \\ \lambda_2 & \lambda_2 & 0 & 0 & 0 \\ \lambda_3 & \lambda_3 & 0 & 0 & 0 \end{bmatrix}.$$

$E^0_{M+/-}$ are the energies of the bare (uncoupled) $M_{+/-}$ magnon modes, which are supposed to change linearly with the magnetic field B, $E^0_{M_{+/-}} = E^0_M \pm g\mu_B B$, where E^0_M denotes the bare magnon gap at $B = 0$. Similarly, $E^0_{P_1}$, $E^0_{P_2}$, and $E^0_{P_3}$ denote the bare energies of P_i ($i = 1, 2, 3$) phonons. Three parameters, λ_1, λ_2, and λ_3, account for possible different strengths of magnon-phonon coupling to each P_1, P_2, and P_3 phonon excitations. Each of these phonons is, however, coupled with the same strength to both M_- and M_+ magnon branches and each λ_i parameter is assumed to be independent of the strength of the applied magnetic field.

The Hamiltonian (1) was diagonalized using the Bogoluybov transformation [12,46] to obtain the field-dependent energies of the coupled magnon-phonon modes. Those were compared with the experimental data and the parameters E^0_M, $E^0_{P_1}$, $E^0_{P_2}$, $E^0_{P_3}$, λ_1, λ_2, λ_3, and g adjusted for the best agreement using the least-square method. The resulting simulation together with the experimental data are shown in Fig. 3 and the values of the fitting parameters are listed in Table I.

V. DISCUSSION

As shown in Fig. 3, our simplified modeling reproduces the observed energy pattern of the avoided crossings of the M_- magnon branch and three P_1, P_2, and P_3 phonons. The deduced coupling strengths (λ_i lambda parameters) are similar for the hybridization of the magnon with both P_1 and P_3 phonons and somewhat weaker in the case of the P_2 phonon (see Table I). Both (M_-, P_3) and (M_-, P_2) pairs are brought into a strong coupling regime when the M_- magnon and the respective phonons tend to coincide at certain values of the magnetic field: the separation between hybrid modes always surpasses their spectral widths [see Fig. 1(b)]. The same can be expected for the pair of (M_-, P_1) modes, viewing the extracted value of the λ_1 parameter.

The coupling between M_+/M_- and P_i (i = 1,2,3) modes also persists in the absence of magnetic field. As for the phonon modes, this coupling is reflected by the red shift of the experimentally observed resonances with respect to the undressed modes (see Table I). The "renormalization" of the phonon modes is rather small, at the level of few percents of their apparent energies, but is still indicative of the mode hybridization, even in the absence of magnetic field. The magnon-phonon coupling affects also the magnon mode, but in a different way than phonons, i.e., by lifting the two-fold degeneracy of this mode at zero magnetic field (see Fig. 4). The zero-field splitting Δ of the magnon mode, into $M_+{}^*$ and $M_-{}^*$ components, is not resolved in the experimental data presented in Figs. 1(b) and 2. But it is clearly apparent in the spectra shown in Fig. 4(a), and measured with higher spectral resolution in the range of small magnetic fields. In the frame of our model the lifting of the double degeneracy of the magnon mode is a consequence of its hybridization with

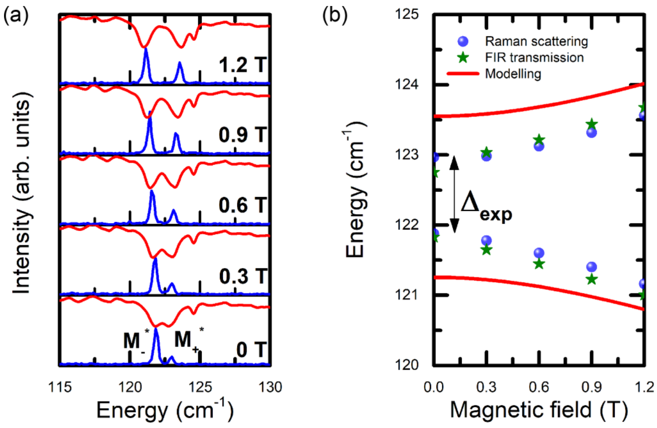

FIG. 4. (a) High-resolution magneto-Raman scattering and FIR transmission spectra of magnon resonance measured at low magnetic fields from 0 to 1.2 T. The transmission minimum, slightly above M_+^* resonance, is only visible in FIR spectra measured under high resolution and is unaffected by the magnon excitation. (b) Energies of the two components of the magnon mode as a function of the magnetic field, extracted from the spectra shown in (b) together with the results of data simulation (solid lines) applied to reproduce the evolution of hybrid magnon-phonon modes in the full range of magnetic field investigated (see Fig. 3).

phonons of lower energies: two initially degenerate magnon states split into their symmetric and antisymmetric combinations. The energy of lower-energy antisymmetric component $M_-{}^*$ is, in fact, not affected by the coupling and corresponds to the bare magnon mode. The upper symmetric $M_+{}^*$ component is shifted up in energy by an amount of Δ. As illustrated in Fig. 4(b), $\Delta \approx 1$ cm^{-1} is derived from the experiment. This value is smaller, by a factor of 2, from the one extracted from our calculation, which can signify the limitation of our simple phenomenological model. We have, for example, checked that imposing certain coupling (strength up to $\lambda = 2$ cm^{-1}) of the magnon mode with the higher-energy P_4 phonon does not practically change the quality of data simulation presented in Fig. 3. But it can suppress the amplitude of Δ closer to its experimental value. It is logical to assume that the zero-field spitting we observe for the magnon-gap excitation in $FePS_3$ is a consequence of the apparent magnon-phonon interaction in this material. We note that such splitting may also be driven by other mechanisms, including those referring to purely magnetic interactions [47,48]. This, in combination with our findings, calls for further revision of antiferromagnetism in $FePS_3$, with theoretical studies in particular.

Having established the characteristic behavior of the energy spectrum of coupled magnon-phonon modes, we now turn to the discussion of the uncommon optical selection rules. They mediate the observation of these modes in our spectra. Focusing first on the magnon excitation and on its Raman scattering response, we confirm that the selection rules, established a long time ago [49] for the conventional MnF_2 and FeF_2 antiferromagnets, cannot strictly be applied to the case of $FePS_3$ [24]. Certain dichroism in the magneto-Raman scattering remains apparent. As demonstrated in Ref. [42], the observation of the M_+ (M_-) branch is favored in the configuration of circularly cross-polarized (copolarized) beams of the excitation and scattered light. On the other hand, as also shown in Ref. [42], the $M_-{}^*/M_+{}^*$ zero-field components of the magnon excitation display the characteristic Raman selection rules when probed under conditions of differently oriented linear polarization of the excitation and scattered light. Other observations which bring our particular attention are the following. (a) Magnon and $P_i = 1{,}2{,}3$ phonon resonances are apparent in both Raman scattering as well as in photon absorption processes. Whereas the conventional selection rules are usually different for those two processes, at least in reference to phonon resonances. (b) Magnon excitation raises a strong absorption resonance (as seen in FIR transmission spectra), although the unit cell of $FePS_3$ is commonly assumed to preserve the inversion symmetry in the antiferromagnetic phase [50]. Thus the magnon-absorption process in this material might not be expected to be active within the electric-dipole approximation. (c) In the absence of magnetic field, i.e., in the regime of weak coupling between M_- magnon and $P_i = 1, 2, 3$ phonon modes, the magnon absorption resonance dominates over those associated to $P_i = 1, 2, 3$ phonons; these phonon resonances gain oscillator strength when they hybridize efficiently with the M_- magnon branch at high magnetic fields. It is tempting to speculate that the effective spin-phonon coupling is at the origin of the above listed observations. This coupling, evidenced here for the characteristic M and P_i excitations, may also be thought to affect the ground state of our antiferromagnetic system, leading to a deformation of the unit cell that breaks its inversion symmetry. With such an assumption, the magnon-excitation can couple to light within the electric-dipole approximation that would account for our observation of a relatively strong magnon resonance in FIR transmission spectra. The P_i phonon excitations apparent in Raman scattering are then presumed to gain oscillator strength via their coupling to the magnon mode. This is in overall agreement with the evolution of the intensities of the P_i absorption resonances when tuning the strength of the magnon-phonon coupling with the applied magnetic field. In fact, the only phonons which are observed to effectively couple to the magnon excitation are those apparent in both Raman scattering and FIR transmission spectra. The above speculations call for their solid verification on the theoretical ground. Nevertheless, our experimental demonstration of the effective optical activity of hybrid magnon-phonon modes in $FePS_3$ antiferromagnet may already be of special importance for future studies of this material in magnon/phonon optical pumping experiments [51].

VI. CONCLUSION

In conclusion, we uncovered the efficient interaction between the magnon and selective phonon modes in $FePS_3$, an archetype of van der Waals, quasi-two-dimensional antiferromagnet. This interaction is revealed with magnetospectroscopy methods, which are uniquely operational in the apparent regime of coupling between the magnon-excitation and the lower-in-energy optical-like phonon modes. The strength of the magnon-phonon coupling is estimated with the clear observation of hybrid magnon-phonon modes, the magnon polarons, when the magnon-gap is shrinked with the applied magnetic field, to intersect the otherwise bare phonon modes. The hybrid magnon-phonon modes in $FePS_3$ are efficiently traced with Raman scattering experiments, but they also directly couple to light, raising the pronounced resonances in FIR transmission spectra. This can be expected to trigger further exploration of $FePS_3$, by probing the magnetization dynamics in this antiferromagnet with THz-pulsed excitation, including the offered possibility to tune the strength of magnon-phonon with an applied magnetic field. We also believe that magnetospectroscopy techniques might be promising in studies of other magnetically ordered systems in which, in particular, the magnon excitations are suspected to couple to lower-energy phonons. Micro-Raman scattering techniques continue to offer an interesting possibility to study magnetism in the ultimate limit of laterally small and strictly two-dimensional systems.

ACKNOWLEDGMENTS

We acknowledge the discussions with Charles Simon, Andrew R. Wildes, Andrés Saúl, Krishnendu Sengupta, and Abhishek Dey. The work has been supported by the EU Graphene Flagship project, CNRS via IRP "2D materials" and the ATOMOPTO project (TEAM programme of the Foundation for Polish Science, co-financed by the EU within the ERDFund). S.M. is grateful to DST-INSPIRE for the fellowship. S.D. acknowledges the financial support from DST-SERB Grant No. ECR/2017/002037 and UGC-DAE CSR Grant No. CRS-M-279. S.D. also acknowledges support from the Technical Research Centre (TRC), IACS, Kolkata. M.V acknowledges the support by the Operational Program Research, Development and Education financed by European Structural and Investment Funds and the Czech Ministry of Education, Youth and Sports (Project MATFUN Grant No. CZ.02.1.01/0.0/0.0/15_003/0000487). The Polish participation in European Magnetic Field Laboratory (EMFL) is supported by the DIR/WK/2018/07.

M. Potemski, S.D., M.O., and C.F. conceived the project and designed the experiments. A.G., S.M., and D.V. prepared the samples and performed their initial characterization together with M. Palit. D.V., M. Palit, J.W., A.D., P.K., A.G., and M.G. performed the experiments and analyzed the data. M.V. proposed and developed the phenomenological model, with contributions from S.G., M.O., and M. Potemski. All authors discussed the results and actively commented on the manuscript written by M. Potemski with the initial input from D.V., M. Palit, and S.D.

[1] R. L. Stamps, S. Breitkreutz, J. Åkerman, A. V. Chumak, Y. Otani, G. E. W. Bauer, J.-U. Thiele, M. Bowen, S. A. Majetich, M. Klaui, I. L. Prejbeanu, B. Dieny, N. M. Dempsey, and B. Hillebrands, The 2014 magnetism roadmap, J. Phys. D **47**, 333001 (2014).

[2] V. Baltz, A. Manchon, M. Tsoi, T. Moriyama, T. Ono, and Y. Tserkovnyak, Antiferromagnetic spintronics, Rev. Mod. Phys. **90**, 015005 (2018).

[3] C. Gong and X. Zhang, Two-dimensional magnetic crystals and emergent heterostructure devices, Science **363**, eaav4450 (2019).

[4] M. Gibertini, M. Koperski, A. F. Morpurgo, and K. S. Novoselov, Magnetic 2D materials and heterostructures, Nat. Nanotechnol. **14**, 408 (2019).

[5] P. Němec, M. Fiebig, T. Kampfrath, and A. V. Kimel, Antiferromagnetic opto-spintronics, Nat. Phys. **14**, 229 (2018).

[6] T. Sekine, M. Jouanne, C. Julien, and M. Balkanski, Light-scattering study of dynamical behavior of antiferromagnetic spins in the layered magnetic semiconductor $FePS_3$, Phys. Rev. B **42**, 8382 (1990).

[7] A. R. Wildes, K. C. Rule, R. I. Bewley, M. Enderle, and T. J. Hicks, The magnon dynamics and spin exchange parameters of FePS3, J. Phys.: Condens. Matter **24**, 416004 (2012).

[8] J.-U. Lee, S. Lee, J. H. Ryoo, S. Kang, T. Y. Kim, P. Kim, C.-H. Park, J.-G. Park, and H. Cheong, Ising-type magnetic ordering in atomically thin $FePS_3$, Nano Lett. **16**, 7433 (2016).

[9] B. L. Chittari, Y. Park, D. Lee, M. Han, A. H. MacDonald, E. Hwang, and J. Jung, Electronic and magnetic properties of single-layer MPX_3 metal phosphorous trichalcogenides, Phys. Rev. B **94**, 184428 (2016).

[10] A. Kamra and G. E. Bauer, Actuation, propagation, and detection of transverse magnetoelastic waves in ferromagnets, Solid State Commun. **198**, 35 (2014).

[11] F. Godejohann, A. V. Scherbakov, S. M. Kukhtaruk, A. N. Poddubny, D. D. Yaremkevich, M. Wang, A. Nadzeyka, D. R. Yakovlev, A. W. Rushforth, A. V. Akimov, and M. Bayer, Magnon polaron formed by selectively coupled coherent magnon and phonon modes of a surface patterned ferromagnet, Phys. Rev. B **102**, 144438 (2020).

[12] H. T. Simensen, R. E. Troncoso, A. Kamra, and A. Brataas, Magnon-polarons in cubic collinear antiferromagnets, Phys. Rev. B **99**, 064421 (2019).

[13] J. Li, H. T. Simensen, D. Reitz, Q. Sun, W. Yuan, C. Li, Y. Tserkovnyak, A. Brataas, and J. Shi, Observation of Magnon Polarons in a Uniaxial Antiferromagnetic Insulator, Phys. Rev. Lett. **125**, 217201 (2020).

[14] S. Streib, N. Vidal-Silva, K. Shen, and G. E. W. Bauer, Magnon-phonon interactions in magnetic insulators, Phys. Rev. B **99**, 184442 (2019).

[15] T. Kikkawa, K. Shen, B. Flebus, R. A. Duine, K.-I. Uchida, Z. Qiu, G. E. W. Bauer, and E. Saitoh, Magnon Polarons in the Spin Seebeck Effect, Phys. Rev. Lett. **117**, 207203 (2016).

[16] A. Pimenov, A. A. Mukhin, V. Y. Ivanov, V. D. Travkin, A. M. Balbashov, and A. Loidl, Possible evidence for electromagnons in multiferroic manganites, Nat. Phys. **2**, 97 (2006).

[17] G. E. W. Bauer, E. Saitoh, and B. J. van Wees, Spin caloritronics, Nat. Mater. **11**, 391 (2012).

[18] D. A. Bozhko, V. I. Vasyuchka, A. V. Chumak, and A. A. Serga, Magnon-phonon interactions in magnon spintronics (review article), Low Temp. Phys. **46**, 383 (2020).

[19] A. V. Chumak, V. I. Vasyuchka, A. A. Serga, and B. Hillebrands, Magnon spintronics, Nat. Phys. **11**, 453 (2015).

[20] J. Walowski and M. Munzenberg, Perspective: Ultrafast magnetism and THz spintronics, J. Appl. Phys. **120**, 140901 (2016).

[21] H. Man, Z. Shi, G. Xu, Y. Xu, X. Chen, S. Sullivan, J. Zhou, K. Xia, J. Shi, and P. Dai, Direct observation of magnon-phonon

coupling in yttrium iron garnet, Phys. Rev. B **96**, 100406(R) (2017).

[22] A. S. Sukhanov, M. S. Pavlovskii, P. Bourges, H. C. Walker, K. Manna, C. Felser, and D. S. Inosov, Magnon-polaron excitations in the noncollinear antiferromagnet Mn_3Ge, Phys. Rev. B **99**, 214445 (2019).

[23] L. Dreher, M. Weiler, M. Pernpeintner, H. Huebl, R. Gross, M. S. Brandt, and S. T. B. Goennenwein, Surface acoustic wave driven ferromagnetic resonance in nickel thin films: Theory and experiment, Phys. Rev. B **86**, 134415 (2012).

[24] A. McCreary, J. R. Simpson, T. T. Mai, R. D. McMichael, J. E. Douglas, N. Butch, C. Dennis, R. Valdés Aguilar, and A. R. Hight Walker, Quasi-two-dimensional magnon identification in antiferromagnetic $FePS_3$ via magneto-Raman spectroscopy, Phys. Rev. B **101**, 064416 (2020).

[25] S. Liu, A. Granados del Águila, D. Bhowmick, C. K. Gan, T. Thu Ha Do, M. A. Prosnikov, D. Sedmidubský, Z. Sofer, P. C. M. Christianen, P. Sengupta, and Q. Xiong, Direct Observation of Magnon-Phonon Strong Coupling in Two-Dimensional Antiferromagnet at High Magnetic Fields, Phys. Rev. Lett. **127**, 097401 (2021).

[26] V. Grasso and L. Silipigni, Low-dimensional materials: The MPX_3 family, physical features and potential future applications, La Riv. Nuovo Cimento **25**, 1 (2002).

[27] B. E. Taylor, J. Steger, and A. Wold, Preparation and properties of some transition metal phosphorus trisulfide compounds, J. Solid State Chem. **7**, 461 (1973).

[28] K. Kurosawa, S. Saito, and Y. Yamaguchi, Neutron diffraction study on $MnPS_3$ and $FePS_3$, J. Phys. Soc. Jpn. **52**, 3919 (1983).

[29] P. A. Joy and S. Vasudevan, Magnetism in the layered transition-metal thiophosphates MPS_3 (M=Mn, Fe, and Ni), Phys. Rev. B **46**, 5425 (1992).

[30] K. C. Rule, G. J. McIntyre, S. J. Kennedy, and T. J. Hicks, Single-crystal and powder neutron diffraction experiments on $FePs_3$: Search for the magnetic structure, Phys. Rev. B **76**, 134402 (2007).

[31] D. Lançon, H. C. Walker, E. Ressouche, B. Ouladdiaf, K. C. Rule, G. J. McIntyre, T. J. Hicks, H. M. Rønnow, and A. R. Wildes, Magnetic structure and magnon dynamics of the quasi-two-dimensional antiferromagnet $FePS_3$, Phys. Rev. B **94**, 214407 (2016).

[32] A. R. Wildes, M. E. Zhitomirsky, T. Ziman, D. Lançon, and H. C. Walker, Evidence for biquadratic exchange in the quasi-two-dimensional antiferromagnet $FePS_3$, J. Appl. Phys. **127**, 223903 (2020).

[33] A. R. Wildes, D. Lançon, M. K. Chan, F. Weickert, N. Harrison, V. Simonet, M. E. Zhitomirsky, M. V. Gvozdikova, T. Ziman, and H. M. Rønnow, High field magnetization of $FePS_3$, Phys. Rev. B **101**, 024415 (2020).

[34] G. Ouvrard, R. Brec, and J. Rouxel, Structural determination of some MPS_3 layered phases (M = Mn, Fe, Co, Ni, and Cd), Mater. Res. Bull. **20**, 1181 (1985).

[35] K.-Z. Du, X.-Z. Wang, Y. Liu, P. Hu, M. I. B. Utama, C. K. Gan, Q. Xiong, and C. Kloc, Weak Van der Waals stacking, wide-range band gap, and Raman study on ultrathin layers of metal phosphorus trichalcogenides, ACS Nano **10**, 1738 (2016).

[36] M. Scagliotti, M. Jouanne, M. Balkanski, G. Ouvrard, and G. Benedek, Raman scattering in antiferromagnetic $FePS_3$ and $FePSe_3$ crystals, Phys. Rev. B **35**, 7097 (1987).

[37] A. Ghosh, M. Palit, S. Maity, V. Dwij, S. Rana, and S. Datta, Spin-phonon coupling and magnon scattering in few-layer antiferromagnetic $FePS_3$, Phys. Rev. B **103**, 064431 (2021).

[38] M. Balkanski, M. Jouanne, G. Ouvrard, and M. Scagliotti, Effects due to spin ordering in layered MPX_3 compounds revealed by inelastic light scattering, J. Phys. C: Sol. State Phys. **20**, 4397 (1987).

[39] A. Hashemi, H.-P. Komsa, M. Puska, and A. V. Krasheninnikov, Vibrational properties of metal phosphorus trichalcogenides from first-principles calculations, J. Phys. Chem. C **121**, 27207 (2017).

[40] X. Wang, K. Du, Y. Y. F. Liu, P. Hu, J. Zhang, Q. Zhang, M. H. S. Owen, X. Lu, C. K. Gan, P. Sengupta, C. Kloc, and Q. Xiong, Raman spectroscopy of atomically thin two-dimensional magnetic iron phosphorus trisulfide ($FePS_3$) crystals, 2D Mater. **3**, 031009 (2016).

[41] F. Kargar, E. A. Coleman, S. Ghosh, J. Lee, M. J. Gomez, Y. Liu, A. S. Magana, Z. Barani, A. Mohammadzadeh, B. Debnath, R. B. Wilson, R. K. Lake, and A. A. Balandin, Phonon and thermal properties of quasi-two-dimensional $FePS_3$ and $MnPS_3$ antiferromagnetic semiconductors, ACS Nano **14**, 2424 (2020).

[42] See Supplemental Material at http://link.aps.org/supplemental/10.1103/PhysRevB.104.134437 for more details on FIR magnetotransmission response (identification of particular phonon resonances and the upper magnon mode) as well as on magneto-Raman scattering data (circular and linear polarization resolved spectra and response in Voigt geometry).

[43] M. Bernasconi, G. L. Marra, G. Benedek, L. Miglio, M. Jouanne, C. Julien, M. Scagliotti, and M. Balkanski, Lattice dynamics of layered MPX_3 (M=Mn,Fe,Ni,Zn; X=S,Se) compounds, Phys. Rev. B **38**, 12089 (1988).

[44] C. Murayama, M. Okabe, D. Urushihara, T. Asaka, K. Fukuda, M. Isobe, K. Yamamoto, and Y. Matsushita, Crystallographic features related to a van der Waals coupling in the layered chalcogenide $FePS_3$, J. Appl. Phys. **120**, 142114 (2016).

[45] K. A. Hay and J. B. Torrance, Magnon-phonon interaction observed in far infrared studies of $FeCl_2.2H_2O$ and $CoCl_2.2H_2O$, J. Appl. Phys. **40**, 999 (1969).

[46] R. M. White, M. Sparks, and I. Ortenburger, Diagonalization of the antiferromagnetic magnon-phonon interaction, Phys. Rev. **139**, A450 (1965).

[47] M. I. Kobets, K. G. Dergachev, S. L. Gnatchenko, E. N. Khats'ko, Y. M. Vysochanskii, and M. I. Gurzan, Antiferromagnetic resonance in $Mn_2P_2S_6$, Low Temp. Phys. **35**, 930 (2009).

[48] K. Shen, Magnon Spin Relaxation and Spin Hall Effect Due to the Dipolar Interaction in Antiferromagnetic Insulators, Phys. Rev. Lett. **124**, 077201 (2020).

[49] P. A. Fleury and R. Loudon, Scattering of light by one- and two-magnon excitations, Phys. Rev. **166**, 514 (1968).

[50] V. N. Krivoruchko, Electrically active magnetic excitations in antiferromagnets (review article), Low Temp. Phys. **38**, 807 (2012).

[51] H. Hayashi and K. Ando, Spin Pumping Driven by Magnon Polarons, Phys. Rev. Lett. **121**, 237202 (2018).